JVI Journals.ASM.org

Herpes Simplex Virus Membrane Proteins gE/gI and US9 Act Cooperatively To Promote Transport of Capsids and Glycoproteins from Neuron Cell Bodies into Initial Axon Segments

Paul W. Howard, Tiffani L. Howard, David C. Johnson

Department of Molecular Microbiology and Immunology, Oregon Health & Science University, Portland, Oregon, USA

Herpes simplex virus (HSV) and other alphaherpesviruses must move from sites of latency in ganglia to peripheral epithelial cells. How HSV navigates in neuronal axons is not well understood. Two HSV membrane proteins, gE/gI and US9, are key to understanding the processes by which viral glycoproteins, unenveloped capsids, and enveloped virions are transported toward axon tips. Whether gE/gI and US9 function to promote the loading of viral proteins onto microtubule motors in neuron cell bodies or to tether viral proteins onto microtubule motors within axons is not clear. One impediment to understanding how HSV gE/gI and US9 function in axonal transport relates to observations that gE$^-$, gI$^-$, or US9$^-$ mutants are not absolutely blocked in axonal transport. Mutants are significantly reduced in numbers of capsids and glycoproteins in distal axons, but there are less extensive effects in proximal axons. We constructed HSV recombinants lacking both gE and US9 that transported no detectable capsids and glycoproteins to distal axons and failed to spread from axon tips to adjacent cells. Live-cell imaging of a gE$^-$/US9$^-$ double mutant that expressed fluorescent capsids and gB demonstrated >90% diminished capsids and gB in medial axons and no evidence for decreased rates of transport, stalling, or increased retrograde transport. Instead, capsids, gB, and enveloped virions failed to enter proximal axons. We concluded that gE/gI and US9 function in neuron cell bodies, in a cooperative fashion, to promote the loading of HSV capsids and vesicles containing glycoproteins and enveloped virions onto microtubule motors or their transport into proximal axons.

Alphaherpesviruses depend upon highly evolved mechanisms to move from mucosal epithelial tissues within neuronal axons to ganglia where latency is established. Following reactivation from latency, virus particles move from ganglia back to peripheral tissues for spread to other hosts. This anterograde transport involves fast axon transport involving microtubules and kinesin motors that propel viral particles from neuron cell bodies (in ganglia) over large distances to axon tips.

Depending upon the strain of alphaherpesvirus and the type of neuron, anterograde transport can apparently involve either fully assembled virions or unenveloped capsids (reviewed in references1, 2, and3). Fully assembled, enveloped virions or "Married" particles (4) are produced by capsid envelopment in the cytoplasm of neuron cell bodies, while "Separate" (4) unenveloped capsids (lacking viral glycoproteins) become enveloped at or near axon tips. Early electron microscopy (EM) studies produced evidence for Separate herpes simplex virus (HSV) capsids in human and rat neuronal axons (5–7). Other, more recent EM studies observed a mixture of Separate capsids (25%) and Married particles for two HSV strains (8), but this ratio was reversed, so that 70% of the particles in axons were Separate particles with another HSV strain (T. Mettenleiter, personal communication). Our antibody staining of HSV-infected human neuroblastoma cells produced evidence for mainly Separate capsids and distinct glycoprotein-containing vesicles (4, 9, 10). EM and fluorescent protein analyses of pig pseudorabies virus (PRV) strongly support only Married transport (11–14). A study involving a "two-color" HSV recombinant expressing a fluorescent glycoprotein and capsids concluded that most HSV anterograde transport involved Married particles (15). Using another "two-color" HSV recombinant expressing fluorescent capsids and glycoproteins gB, we concluded that a majority of capsids moving in rat superior cervical ganglion (SCG) neurons were Separate particles (60%) (16). Thus, we believe that both modes of transport are possible and, in fact, occur.

HSV and PRV express two membrane proteins, gE/gI and US9, which are key to the understanding of anterograde transport in neuronal axons (reviewed in references 2 and3). gE/gI is a heterodimer, with both gE and gI required for function, and possesses both substantial extracellular domains and ~100-amino-acid (aa) cytoplasmic domains with acidic clusters, dileucine, and tyrosine motifs that cause the protein to extensively localize to the trans-Golgi network (TGN) (17–20). HSV and PRV US9 proteins are type II membrane proteins, tail anchored, with no significant extracellular domains and cytoplasmic domains that also contain TGN localization motifs (21–24).

We previously demonstrated that HSV gE/gI and US9 promote the anterograde transport of both viral glycoproteins (gB and gD) and Separate capsids (4). Given that gE/gI and US9 are membrane proteins yet influence the transport of unenveloped capsids (apparently without membranes), we proposed the "loading hypothesis" (4). In this model, gE/gI and US9 localize to TGN membranes and promote the accumulation of other viral membrane and tegument proteins in the TGN (depicted in Fig. 1A). By this accumulation, gE/gI and US9 together collect viral proteins into

Received 11 September 2012 **Accepted** 13 October 2012

Published ahead of print 17 October 2012

Address correspondence to David C. Johnson, johnsoda@ohsu.edu.

Supplemental material for this article may be found at http://dx.doi.org/10.1128/JVI.02465-12.

doi:10.1128/JVI.02465-12

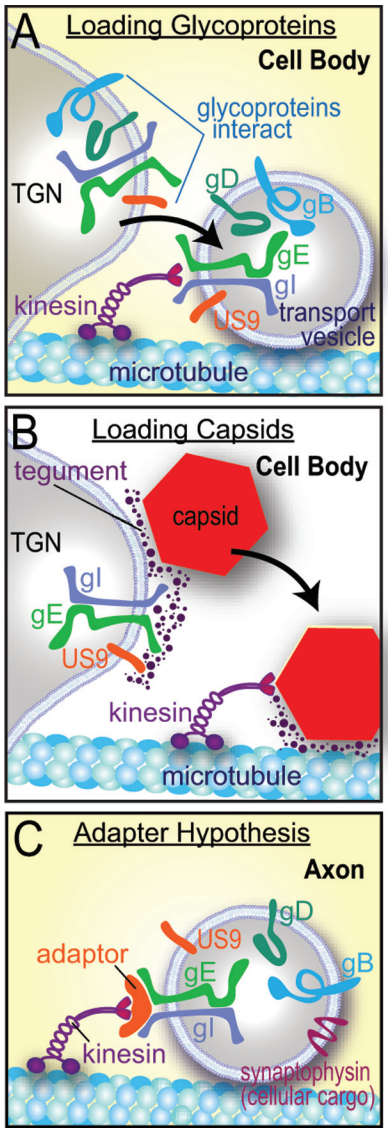

FIG 1 Models for how HSV gE/gI and US9 might promote anterograde axonal transport of capsids and glycoproteins. (A) The loading hypothesis suggests that gE/gI and US9 accumulate in the TGN of neuron cell bodies and cause other HSV membrane proteins to accumulate there. Transport vesicles that bud from these specific TGN membranes are loaded onto kinesins for transport into proximal axons. Similar vesicles containing enveloped HSV (Married) particles might also be loaded in this way. (B) The loading of capsids onto kinesin motors may similarly be affected by gE/gI and US9 accumulation in the TGN. gE/gI is known to extensively interact with tegument proteins that, in turn, interact with capsids. Thus, by causing the accumulation of capsids in TGN loading compartments, gE/gI and US9 may promote the axonal transport of unenveloped capsids. (C) The adaptor hypothesis functions more extensively in axons rather than cell bodies. In this model, the cytoplasmic domains of gE/gI and US9 interact with kinesin adaptors or directly with kinesins to tether vesicles containing other HSV glycoproteins (gD and gB) and cellular cargo (synaptophysin) onto motors during transport.

vesicles that are subsequently loaded onto kinesin motors (Fig. 1B). In this model, the TGN serves as a platform and sorting machinery for the assembly of transport vesicles onto kinesin motors that subsequently transport in axons. To explain how gE/gI and US9, membrane proteins, might increase the axonal transport of Separate capsids, we note that gE/gI interacts extensively with tegument proteins that are encrusted on the surfaces of capsids (2, 25–28). An alternative hypothesis, which might explain how gE/gI and US9 promote the transport of HSV structural proteins, was termed the "adaptor hypothesis." In this model, the relatively large cytoplasmic domains of gE/gI and US9 promote the tethering of HSV glycoprotein-laden vesicles onto adaptors or kinesins, maintaining the transport along axons (depicted in Fig. 1C) (reviewed in reference 2).

One problem in testing these two hypotheses relates to observations that HSV gE-, gI-, or US9-null mutants do not exhibit a total block in anterograde transport of capsids and glycoprotein-containing vesicles. When the numbers of capsids and glycoproteins were quantified in distal axons, gE^-, gI^-, and $US9^-$ mutants often exhibited 5- to 10-fold reductions in the numbers of capsids and glycoproteins in distal axons, but only infrequently were there no distal puncta (4). Moreover, in proximal axons, the reductions in numbers puncta associated with the loss of gE, gI, or US9 were much lower. Similar observations have been made with PRV gE^-, gI^-, and $US9^-$ mutants (29, 30). Observations of reduced transport of alphaherpesvirus proteins, especially in more distal axons, support the adaptor hypothesis. However, there were also decreased numbers of capsids and glycoproteins in the most proximal regions of axons, supporting the loading hypothesis.

The understanding of how HSV gE/gI and US9 function in neurons has, in some cases, been blurred because some investigations have not considered that gE/gI and US9 can potentially play two roles in virus spread: (i) anterograde transport of virus particles from neuron cell bodies to axon tips and (ii) extracellular spread of virus from the surfaces of neuronal axons to adjacent cells. For example, McGraw et al. (31) concluded that HSV US9 is dispensable for anterograde spread, while gE/gI is essential for spread. In these studies, HSV spread was measured from neuron cell bodies isolated in Campenot chambers to axon tips, followed by infection of adjacent Vero cells and measuring virus produced by these Vero cells. Two HSV $US9^-$ mutants produced 10- to 100-fold less infectious virus in Vero cells after 24 h than repaired viruses, although after 48 h, the differences were less. Early time points better represent HSV transport in axons and spread, because virus is massively amplified in Vero cells. To us, these results showed that US9 is important for HSV anterograde transport and spread. Important to consider is that the results did not specifically measure anterograde transport but instead represented the sum total of anterograde transport, extracellular spread from neurons to Vero cells, infection of Vero cells, and then spread between Vero cells.

To try to better understand how HSV gE/gI and US9 function, whether by the adaptor versus loading model, we used two approaches. First, we constructed two different HSV recombinants lacking both gE and US9 in order to test whether these proteins had overlapping or redundant functions in axonal transport. One of these mutants expressed fluorescent capsids and glycoproteins. Second, we used neurons growing in microfluidic chambers (32), which allowed us to perform live-cell imaging of fluorescent capsids and glycoproteins produced by gE^-, $US9^-$, and $gE^-/US9^-$ mutant viruses in medial and distal axons that were isolated from neuron cell bodies. As before, HSV mutants lacking just gE or US9 transported quantitatively reduced numbers of both capsids and glycoprotein gB to distal axons. However, $gE^-/US9^-$ double mutants transported no detectable capsids and gB puncta to distal axons, and there was no infection of adjacent nonneuronal cells.

Live-cell imaging of fluorescent capsids and gB in medial and proximal axons showed that the loss of both gE and US9 substantially (>90%) reduced the numbers of capsids and glycoproteins in axons. The results largely supported the loading hypothesis, although there was also some evidence supporting the adaptor hypothesis.

MATERIALS AND METHODS

Cells and viruses. Vero cells were grown in Dulbecco's modified Eagle's medium (D-MEM) containing 10% fetal bovine serum and used to propagate and determine the titer of HSV. F-gE/GFP and F-gE/GFP-R (a repaired virus) (33) as well as F-US9/GFP and FUS9/GFP-R (repaired) (24) were all derived from HSV-1 strain F.

Neuronal cell cultures. Superior cervical ganglia (SCG) were dissected from day 18 embryos removed from pregnant Sprague-Dawley rats and dissociated by incubation in 0.25% trypsin in Hibernate A medium (lacking calcium; Brainbits) at 37°C for 10 min. Ganglia were then incubated in 1% soy bean trypsin inhibitor in Hibernate A medium lacking Ca for 5 min at 37°C and then transferred into Neurobasal medium supplemented with 2% B27 containing 50 ng/ml murine nerve growth factor (NGF) 2.5S subunit (all from Invitrogen). Ganglia were then mechanically dissociated by repeated passage through a fire-polished Pasteur pipette. Cells were counted and plated in microfluidic devices (Xona Microfluidics) that were mounted onto glass coverslips or glass-bottomed 35-mm dishes (32, 34). Glass surfaces were prepared by overnight incubation in poly-D-lysine (1 mg/ml) in 0.1 M Na-borate (pH 8.5). The glass was washed twice in water, dried, and then incubated for 2 h in poly-D-lysine (30 μg/ml)–laminin (2 μg/ml) in phosphate-buffered saline (PBS). Glass was then washed twice in water and air dried. SND450 (Xona) microfluidic devices were used for studies involving spread into axonal compartments and spread assays, and ~40,000 SCG neurons were plated in the somal compartments. RD450 microfluidic devices were used for live cell-imaging in somal compartments and involved ~15,000 neurons. Two days after neurons were plated into microfluidic devices, cytosine arabinoside (AraC) (2 μM) was added to the medium in somal compartments to kill non-nonneuronal cells, and after 2 days, the medium was changed. Neurons were infected by adding HSV to somal compartments after 6 or 7 days in culture. For experiments measuring HSV spread to nonneuronal cells, 40,000 Vero cells were plated in the axonal compartments of microfluidic devices 24 h before infection. Human gamma globulin (0.1%) (a source of HSV-neutralizing antibodies) was added to the axonal compartments at the time of virus addition to the somal compartments.

Construction of HSV lacking both gE and US9 genes. An HSV-1 mutant, denoted F-gE/US9/GFP, in which both the gE (US8) and US9 genes were replaced with enhanced green fluorescent protein (EGFP) sequences, was constructed. Homology arms were constructed by PCR encompassing ~1,000 bp 5′ of the gE initiation codon and ~1,125 bp 3′ of the US9 stop codon. These homology arms were inserted upstream and downstream of EGFP sequences in plasmid pEGFP-C1 (Clontech). This plasmid was cotransfected with DNA derived from HSV-1 F-infected cells into Vero cells by using the calcium phosphate technique (35). Viruses that expressed EGFP were selected and plaque purified three times, viral DNA was sequenced, and a virus (F-gE/US9/GFP) was used in all studies described below. A repaired form of F-gE/US9/GFP was constructed by cotransfecting DNA derived from F-gE/US9/GFP viral DNA with a plasmid (pUC18-7,8,9) containing the wild-type sequence for gI, gE, and US9. Viruses which did not express EGFP were selected and plaque purified three times, and this repaired virus was denoted F-gE/US9/GFP-R.

Construction of HSV recombinants that express fluorescent capsids and glycoprotein gB and with deletions in gE, US9, or gE and US9. HSV-1 strain F DNA in the form of a bacterial artificial chromosome (BAC) and encoding monomeric red fluorescent protein (mRFP1) fused to the N terminus of the small capsid protein VP26 and EGFP fused after the signal peptide of gB was described previously (36). This BAC was a kind gift of Greg Smith (Northwestern University Feinberg School of Medicine, Chicago, IL) and had been used to produce an HSV recombinant virus, denoted GS2843, that expresses mRFP-VP26 capsids and EGFR-labeled gB (36). We inserted a kanamycin resistance gene cassette (Kan^r) flanked by FLP recombination target (FRT) sites into the gE, US9, or gE and US9 coding sequences of this BAC using standard recombineering techniques in bacteria, as previously described (37). Homology arms were constructed using PCR so that sequences upstream and downstream of the gE or US9 open reading frames were fused onto Kan^r sequences using the following primers: GGGTTGGTGCGGTGCTGTTTGTTGGG CTCCCATTTTACCCGAAGATCGGCTGCTATCCCC and AACAGGG AGGGGGCGTCGACAGCCTGGAGGGCCATCGGGGAGACAACGGC CGTGTAGCCC for ΔgE and ATTAAAAATCGTGAGTCACTGCGACC GCAACTTCCCACCCGGAGCTTTCTTCCGGCCTCG and TTGCGGG GTGATGGGGGGGAAGAGAGACGACAAGAAGGACGCGCGTGTCG ATGCGGTCTT for ΔUS9.

To construct the ΔgE ΔUS9 double mutant, the 5′ gE homology arm described above was used in conjunction with the 3′ US9 homology arm. The resulting PCR products (containing Kan^r sequences inserted into gE or US9 or both gE and US9 sequences) were electroporated into EL250 bacteria harboring the GS2843 BAC. Recombinant bacteria were selected by plating onto agar plates containing chloramphenicol and kanamycin, and DNA sequences in multiple clones were PCR amplified and sequenced. The kanamycin cassette was collapsed in these BACs by inducing FLP recombinase into bacteria and growing bacteria on medium containing arabinose, producing BACs with the gE, US9, or both gE and US9 genes replaced with ~50 bp of DNA containing one FRT site. Sequences around the gE and US9 genes were amplified by PCR and sequenced. BACs were transfected into Vero cells by using Lipofectamine 2000 (Invitrogen). Two independent BAC clones for each virus were used to produce virus stocks, denoted GS2843, GS2843ΔgE, GS2843ΔUS9, and GS2843ΔgEΔUS9, and each stock was plaque purified 3 times and then characterized for anterograde transport.

Antibodies. Rabbit anti-VP26 antibody was kindly provided by Prashant Desai (Johns Hopkins University, Baltimore, MD). Mouse monoclonal antibody (MAb) specific for ICP4 (58S) was kindly provided by Roger Everett (University of Glasgow Centre for Virus Research, Scotland, United Kingdom). Mouse anti-gB MAb (SS10) and anti-gD MAb (DL6) were kindly provided by Gary Cohen (University of Pennsylvania, Philadelphia, PA). Rabbit anti-US9 antipeptide polyclonal serum was previously described (4). Mouse anti-gE MAb (3114) and anti-gI MAb (3104) were gifts from Howard Marsden (MRC Virology Unit, Glasgow, Scotland, United Kingdom) and were described previously (38). Mouse anti-VP5 MAb was obtained from Virusys (North Berwick, ME). A guinea pig anti-tau antibody was obtained from Synaptic Systems. Rabbit anti-extracellular signal-regulated kinase 1 (ERK-1) antibody was obtained from Santa Cruz Biotechnology. DyLight fluorescent secondary antibodies were obtained from Jackson ImmunoResearch.

Immunofluorescence microscopy of HSV-infected neurons in axonal chambers and counts of viral capsids and gB puncta. Microfluidic chambers containing SCG neurons and, in spread experiments, Vero cells were disassembled and fixed in 4% paraformaldehyde for 10 min at 20°C, permeabilized in 0.1% Triton X-100 for 10 min, and incubated with primary antibodies in PBS containing 0.1% Tween 20 and 2% normal donkey serum. The cells were washed in PBS containing 0.1% Tween 20 and incubated with secondary fluorescent antibodies in PBS containing 0.1% Tween 20 and 2% normal donkey serum. Microscopy was performed at the Oregon Health and Sciences University Advanced Light Microscopy Core using a Deltavision CoreDV Widefield Deconvolution system. Images were captured with a 60× (numerical aperture, 1.42) Plan Apo N objective in three channels, 488 nm, 549 nm, and 649 nm. For the quantification of VP26 and gB puncta, 10 10,551-μm^2 images per slide were captured, with a minimum of six 0.3-μm *z* sections. After deconvolution, the images were processed with the ImageJ program. For VP26 and gB, an intensity threshold of 1,500 and a minimum punctum area of 7 square

pixels (6.4×10^{-3} μm^2) were chosen by comparing manual counts of gB and capsid puncta in several representative images using the softWoRxs Explorer program from Applied Precision and comparing these to the ImageJ software counts (using the Analyze Particles function). Counts of capsid and glycoprotein puncta produced by using ImageJ software were corrected based on the total area of axons in each axonal compartment measured using tau-specific antibodies to stain axons. In other experiments, SCG neurons were infected with GS2843 or mutants derived from this recombinant virus, and fluorescent capsids were manually counted in axonal chambers without fixation or following fixation with cold 50% acetone–50% methanol for 15 min and staining with anti-VP5 MAb.

Live-cell imaging of rat SCG axons in microfluidic chambers. Rat neurons in microfluidic chambers were infected with HSV (8 PFU/cell) for 20 to 24 h and were subjected to live-cell imaging at 37°C under 6% CO_2 in an enclosed chamber using an inverted objective and the deconvolution system described previously (16). Images were acquired as optical axis images in a 512-by-512 binning-of-2 format with a 60× (numerical aperture, 1.42) Plan Apo N objective in 2 colors, green fluorescent protein (GFP) and mRFP. Axons or cell bodies were imaged for a total of 2 min, taking exposures in both channels every 2 s. Images were deconvolved using softWoRxs Explorer software from Applied Precision.

Analyses of HSV replication in SCG neurons. SCG neurons were prepared as described above and plated into 24-well tissue culture dishes (80,000 cells/well) coated with poly-D-lysine and laminin and then with AraC, as described above. Six days after plating, the cells were infected with HSV at 5 PFU/cell. After 2 h, the cells were washed once in Neurobasal medium, and some cells and media were immediately harvested (2-h time point), while other dishes were incubated for 16 to 32 h. In each case, cells were scraped off the plastic dishes into cell culture medium, this mixture was frozen and sonicated, and virus titers were determined using Vero cells. These experiments were performed in triplicate.

Immunoblotting. For Western blot analysis, Vero cells were infected with HSV at 10 PFU/cell for 16 h, the cells were washed once with PBS and collected by scraping into PBS, cells were pelleted, and pellets were suspended in lysis buffer containing 50 mM Tris (pH 8.0), 150 mM NaCl, 1% NP-40, and 1 mM EDTA for 10 min on ice. Insoluble debris was removed by centrifugation at 2,000 × *g* for 5 min; proteins were then denatured using 2% sodium dodecyl sulfate (SDS)–2% β-mercaptoethanol; and the proteins were separated using polyacrylamide gels and then transferred onto polyvinylidene difluoride (PVDF) membranes (Millipore). Membranes were blocked in a solution containing 50 mM Tris-HCl (pH 7.5), 150 mM NaCl, 0.1% Tween 20, and 5% nonfat milk; washed; incubated with primary antibody blots; and then washed and incubated with horseradish peroxidase-conjugated secondary antibody (Santa Cruz). A chemiluminescent reagent was then added, as recommended by the supplier (PerkinElmer).

RESULTS

Construction of an HSV-1 recombinant unable to express both gE and US9. We previously described HSV-1 strain F recombinants in which gE, gI, or US9 sequences were replaced with GFP (4, 24, 33). There were no major defects in the replication of these recombinants in neurons, but the loss of gE, gI, or US9 quantitatively reduced anterograde transport of both capsids and glycoproteins, especially in distal axons (4). These previous studies involved a human neuroblastoma cell line differentiated to produce axons or neurites of 20 to 30 μm. To further investigate the models described in Fig. 1, we constructed a double mutant, denoted F-gE/US9/GFP, by replacing both the gE (US8) and US9 genes with a GFP expression cassette. Note that this mutant was also missing the US8.5 gene (39), which has unknown functions and is not normally considered in these types of studies. To characterize the expression of gE/gI, gD, and US9, Vero cells were infected with mutant viruses, and cell extracts were subjected to Western blot analysis. As expected, F-gE/GFP failed to express gE, and F-US9/GFP failed to express US9 (Fig. 2). F-gE/US9/GFP did not express both gE and US9. Importantly, the expression levels of both gI (encoded by the adjacent US7 gene) and gD (encoded by the US6 gene) were normal in the double mutant. A repaired virus, F-gE/US9/GFP-R, was constructed by cotransfecting Vero cells with F-gE/US9/GFP viral DNA and plasmid DNA containing wild-type US7, US8, and US9 sequences, followed by the selection of nonfluorescent plaques. Sequencing of the US8 and US9 genes of this repaired virus showed the acquisition of gE and US9 sequences (not shown), and this repaired virus expressed gE and US9 (Fig. 2).

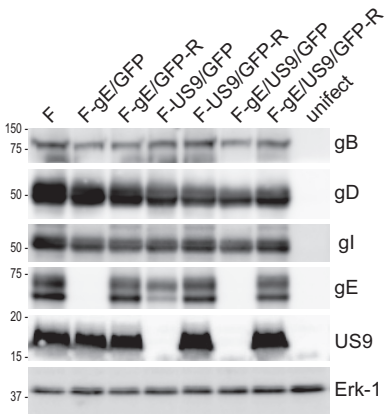

FIG 2 Expression of gE and US9 in cells infected with HSV mutant viruses. Vero cells were infected with wild-type HSV strain F; the gE$^-$, US9$^-$, or gE$^-$/US9$^-$ mutant; or repaired versions of these viruses for 16 h, and SDS-containing cell extracts were then produced. These extracts were resolved on polyacrylamide gels, proteins were transferred onto PVDF membranes, and the membranes were incubated with antibodies specific for gB, gD, gI, gE, US9, or the cellular protein ERK-1. Membranes were washed and incubated with horseradish peroxidase-conjugated secondary antibodies and a chemiluminescent reagent. Numbers indicate molecular mass markers in kilodaltons.

We characterized the replication of these mutants in rat SCG neurons derived from day 18 embryos, as described previously (16, 30). Importantly, these neurons produce much longer axons than SK-N-SH neurons, and the derivation of these axons is robust; i.e., the axons grow up into microfluidic chambers for a more accurate study of transport (see below). Previous studies by us (4) and others (31, 40) have indicated that HSV mutants lacking gE, gI, or US9 produced relatively normal quantities of infectious virus in neurons, although there have been small decreases in yields of virus or kinetics of virus growth. The defects did not account for the marked defects in anterograde transport. Figure 3 shows that F-gE/GFP, F-US9/GFP, F-gE/US9/GFP, and F-gE/US9/GFP-R all produced 8×10^3 to 20×10^3 PFU/ml in the combined cell and cell culture supernatants. It should be noted that we visually confirmed that our neuronal cultures contained no detectable nonneuronal cells after treatment of the SCG neurons for 2 days with 2 μM cytosine arabinoside (AraC), conditions that effectively kill all or most dividing cells. In contrast, other studies showed higher titers of HSV (10^5 PFU/ml) (31), a difference that appears to be related to higher proportions of nonneuronal cells and to the use of lower concentrations of AraC for shorter times. Nonneuronal cells produce much more virus than do neurons (data not shown). We also observed that smaller numbers of nonneuronal cells in our cultures allowed us to administer

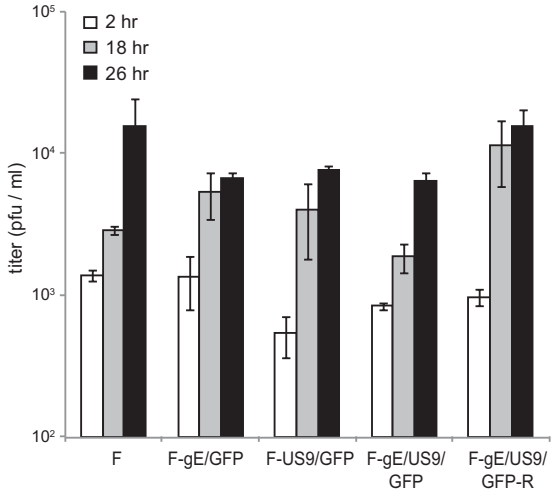

FIG 3 Production of infectious progeny in neurons infected with gE$^-$, US9$^-$, and gE$^-$/US9$^-$ mutants. SCG neurons in 24-well dishes (~40,000 neurons per well) were infected with wild-type HSV strain F; the gE$^-$, US9$^-$, or gE$^-$/US9$^-$ mutant; or repaired viruses at 5 PFU/cell for 2 h, and the cells were then washed once with medium. At this time (2 h) and after 18 and 26 h, the cells were scraped into the medium and then frozen and sonicated, and viral titers were determined using plaque assays involving Vero cells. Each time point was assayed in triplicate, and the data are presented with standard deviations.

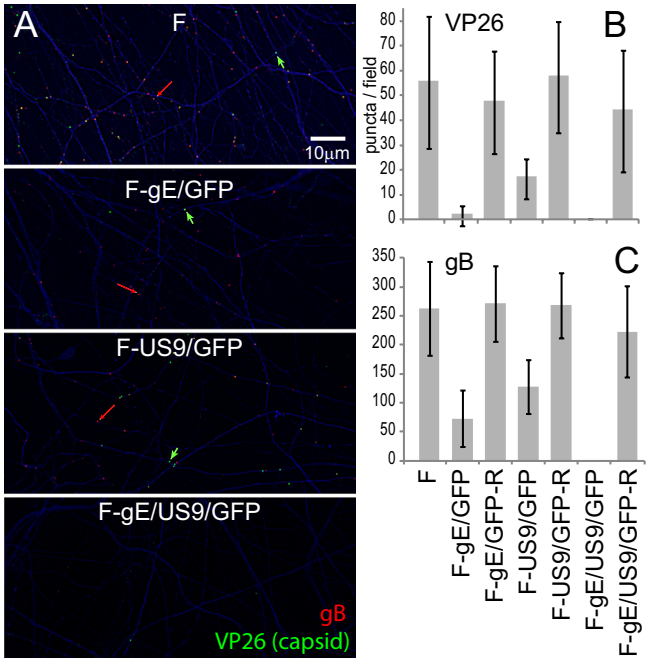

FIG 4 Numbers of capsids and gB puncta in distal axons of SCG neurons infected with the gE$^-$, US9$^-$, or gE$^-$/US9$^-$ mutant. SCG neurons were plated in the somal compartment of microfluidic chambers, and axons were allowed to grow into the axonal side. HSV-1 (8 PFU/cell) was introduced into somal chambers, and 18 h later, the devices were disassembled, and axons in the axonal chambers were fixed with paraformaldehyde and simultaneously immunostained with antibodies specific for VP26 (capsids) (one per panel marked with a green arrow), gB (red) (one per panel marked with a red arrow), and the microtubule-associated protein tau (blue) and then with secondary fluorescent antibodies. (A) Representative images of axons in the axonal compartment. VP26 is stained in green, gB puncta are red, and tau is blue. The puncta were small, and one gB punctum (red) and one VP26 punctum are indicated by arrows. Puncta containing both VP26 and gB (Married particles) appear yellow. (B and C) The ImageJ software program was used to count capsid and gB puncta in 10 distinct 10,551-μm^2 fields of the axonal compartments from three separate infections. Puncta with an intensity of >1,500 and a size of 7 square pixels or greater were counted. The total area of tau staining was also measured and was used to correct the data for the quantities of axons present.

higher doses of HSV (10 PFU/cell), and neurons survived longer, i.e., several days (data not shown). Cultures containing more nonneuronal cells exhibited more cell death with these doses of virus.

HSV gE$^-$ and US9$^-$ mutants exhibited reduced anterograde transport, while a gE$^-$/US9$^-$ double mutant showed no transport. To assess HSV anterograde transport, we used SCG neurons cultured in microfluidic chambers, as described previously (32, 34). These neuron cell bodies growing in somal compartments extend axons through the 450-μm microchannels connecting to axonal compartments, where distal axons and axon tips reside. Hydrostatic pressure prevents diffusion of virus and viral antigens from somal chambers into axonal chambers. In every experiment, Vero cells were plated in the axonal compartments, with no neurons plated in somal compartments, in order to detect any possible virus leakage into axonal compartments. Imaging of axons in microchannels was not compromised by input viral antigens, and there was little or no chance of reinfection of axons, producing retrograde transport of viral proteins. Moreover, the structures of these axons extending through microchannels were highly amenable to live-cell imaging, allowing more accurate assessments of HSV anterograde transport (32).

In order to characterize the culmination of the anterograde transport process, we first enumerated the numbers of capsids and glycoproteins in distal axons found in axonal compartments. SCG neurons were infected in the somal compartments with wild-type or mutant HSV (8 PFU/cell) and then incubated for 18 h. Distal axons present in axonal compartments were simultaneously stained with antibodies specific for VP26 (small capsid protein), gB, and tau (a cellular axon protein). Wild-type HSV-infected neurons displayed numerous capsid puncta (green) and gB puncta (red) within tau-stained axons (Fig. 4A). Axons of neurons infected with either the gE-null virus, F-gE/GFP, or the US9-null mutant, F-US9/GFP, displayed reduced numbers of both capsids and gB puncta. Note that these viruses expressed GFP (from the gene inserted in place of the gE or US9 gene), but this GFP was faint in cell bodies and not detected in axons (not shown). ImageJ software was used to count puncta in axons, using tau staining to control for the numbers of axons present. Variations in the numbers of capsids and gB puncta were relatively large when different microfluidic chambers were compared. However, the results of three experiments showed quantitative reductions in the numbers of capsids and gB puncta in distal axons with gE$^-$ and US9$^-$ viruses, as in our previous report (4). F-gE/GFP exhibited 95%-reduced numbers of capsids and 73%-reduced numbers of gB puncta, compared with wild-type HSV (Fig. 4A and B). F-US9/GFP exhibited 70%-reduced numbers of capsids and 46%-reduced numbers of gB puncta. The repaired viruses F-gE/GFP-R and F-US9/GFP-R transported 102 to 104% of the number of gB puncta and 85 to 103% of the number of capsid puncta (Fig. 4A and B). With wild-type HSV and repaired viruses, there was always 4 to 5 times more gB puncta in terminal axons than capsids. Interestingly, the loss of gE disproportionally affected capsids, so the ratio of gB/capsid puncta with F-gE/GFP was 20 to 25 (Fig. 4A and B).

In contrast to the quantitative reductions in numbers of capsid and gB puncta with the gE- and US9-null viruses, the F-gE/US9/GFP double mutant exhibited not a single VP26 or gB punctum in distal axons in any of the three experiments described above (Fig. 4A and B) or in a fourth experiment comparing just wild-type HSV with F-gE/US9/GFP (not shown). The repaired version of F-gE/US9/GFP, F-gE/US9/GFP-R, transported 89% of gB and 80% of capsid puncta into distal axons. We concluded that gE/gI and US9 each contribute to the axonal transport of both capsids and glycoproteins, but the loss of both gE and US9 abolished transport into distal axons.

Spread of gE$^-$, US9$^-$, and gE$^-$/US9$^-$ mutants from axons to adjacent cells. The extracellular spread of HSV gE$^-$, US9$^-$, and gE$^-$/US9$^-$ mutants from the surfaces of distal axons to other cells was measured by plating Vero cells in the axonal compartments. Sufficient numbers of Vero cells were added so that axon termini were normally in contact with one or more Vero cells. As before, neurons were plated into microfluidic chambers and infected in somal compartments. Human gamma globulin (0.1%) (a source of HSV-neutralizing antibodies) was added to axonal compartments to block HSV spread through the culture medium. Chambers were disassembled after 18 h, the cells were fixed and permeabilized, and Vero cells were then stained with antibodies specific for the HSV immediate-early protein ICP4. We found that it was critical to measure virus spread at early times, 18 h after infection of neurons, in order to focus on the question of whether HSV neuron-to-Vero-cell spread occurred. At later times, 28 to 36 h after infection, there was a massive amplification of virus in Vero cells, which produced much more virus than neurons, so that the vast majority of the viral antigens were derived from other infected Vero cells. Figure 5A shows two Vero cells expressing ICP4 in the nucleus. These Vero cells were in contact with two separate axons (stained with tau antibodies [in blue]). Importantly, other adjacent Vero cells (the monolayer was nearly confluent) did not express ICP4. Thus, at these early times (18 h), there was little HSV spread between Vero cells. Vero cells that were stained with ICP4 antibodies in axonal chambers were counted. Wild-type HSV F and the repaired viruses produced similar levels of ICP4-positive (ICP4$^+$) Vero cells (Fig. 5B). F-gE/GFP and F-US9/GFP were substantially reduced in spread, infecting 12% and 4% of the numbers of Vero cells, respectively, compared to wild-type HSV. The F-gE/US9/GFP double mutant did not spread to a single Vero cells in any of the four experiments (Fig. 5B). Similar results were obtained when human HaCaT keratinocytes were used instead of Vero cells (not shown). These results extended and confirmed the conclusions that there are quantitative reductions in HSV anterograde transport with gE$^-$ and US9$^-$ mutants and that the gE$^-$/US9$^-$ double mutant does not transport either capsids or glycoproteins to distal axons.

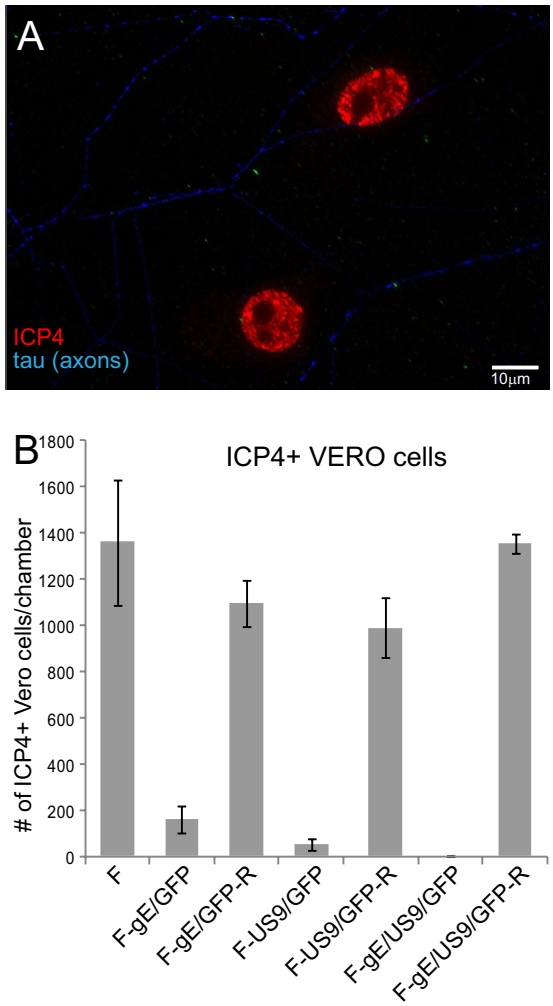

FIG 5 Spread of gE$^-$, US9$^-$, and gE$^-$/US9$^-$ mutants from distal axons to adjacent nonneuronal cells. SCG neurons were plated into microfluidic chambers, and axons were allowed to grow into the axonal compartment. Vero cells were plated in the axonal compartment 24 h before the neurons were infected with HSV-1 (8 PFU/cell) added to the somal compartments. Two to four hours after infection, 0.1% human gamma globulin was added to the axonal chambers, and 18 h after infection, the devices were disassembled. Cells in the axonal chambers were fixed with 4% paraformaldehyde, permeabilized with 0.1% Triton X-100, and immunostained with antibodies specific for the immediate-early gene product ICP4 (red) and simultaneously with antibodies specific for the axon protein tau (blue). (A) Representative image of ICP4$^+$ Vero cells adjacent to two axons stained with tau. (B) ICP4$^+$ Vero cells were manually counted in 10 axonal compartments involving 3 separate experiments. Total numbers of ICP4$^+$ Vero cells per chamber are shown with standard deviations.

Construction of HSV recombinants expressing fluorescent capsids and glycoproteins and lacking gE, US9, or both. To better understand the mechanisms by which gE and US9 promote anterograde transport, it was important to be able to perform live-cell imaging of capsids and glycoproteins in axons. The loading hypothesis depicted in Fig. 1 suggests that the loss of both gE and US9 might produce marked reductions in the quantities of capsids and glycoproteins that enter axons. The adaptor hypothesis suggests that capsids and glycoproteins might be transported into axons, possibly so that there are relatively normal numbers in proximal axons, but viral structures fall off kinesin motors, stall more often, or move with slower kinetics or more frequently in the retrograde direction. To test these models, we constructed three recombinant HSVs derived from a bacterial artificial chromosome (BAC) copy of the HSV strain F genome which includes genes encoding red fluorescent protein (mRFP) fused to the VP26 capsid protein and GFP fused near the N terminus of gB. This BAC was previously constructed and used to derive a dual-fluorescent or "two-color" HSV used to study HSV anterograde transport (15). We used this BAC to derive mutants lacking the gE (US8) gene, the US9 gene, or both the gE and US9 genes, by first replacing the HSV genes with a kanamycin resistance cassette that was

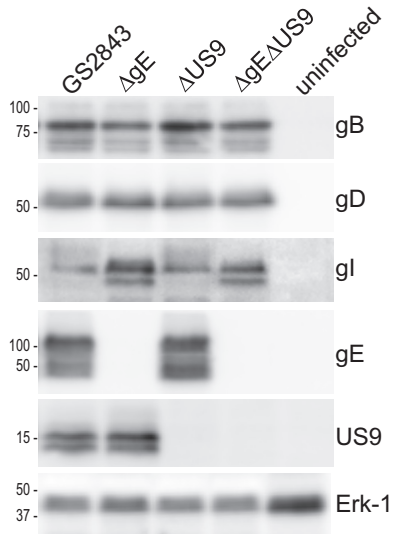

FIG 6 Immunoblot analyses of viral proteins produced by fluorescent HSV recombinants with deletions in the gE, US9, or gE and US9 genes. Vero cells were left uninfected or were infected with HSV recombinant strain GS2843, GS2843ΔgE, GS2843ΔUS9, or GS2843ΔgEΔUS9 for 16 h, and SDS cell extracts were then made, and proteins were resolved on polyacrylamide gels and transferred onto PVDF membranes. The membranes were immunoblotted with antibodies specific for gB, gD, gI, gE, US9, or the cellular protein ERK-1. Numbers represent molecular mass markers in kilodaltons.

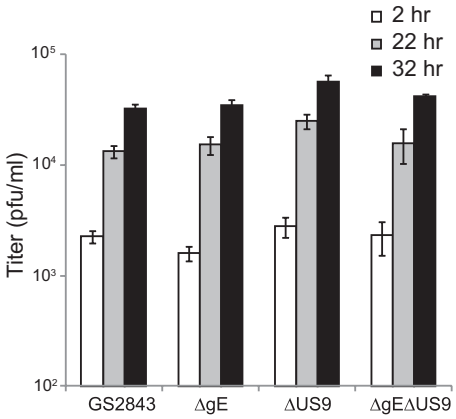

FIG 7 Replication of fluorescent HSV recombinants with deletions in the gE, US9, or gE and US9 genes in neurons. SCG neurons in 24-well plates were infected with GS2843, GS2843ΔgE, GS2843ΔUS9, or GS2843ΔgEΔUS9 at 5 PFU/cell. After 2 h, cells were washed once with medium. Cells and medium were harvested immediately (2 h) or after 22 or 32 h and then frozen and subsequently sonicated, and the viral titers were then determined using Vero cells. Each time point represents three separate wells, and the data are presented as the averages with standard deviations.

flanked by FRT sites. The kanamycin cassette was subsequently removed from the BACs by inducing FLP recombinase so that ~50 bp replaced US8, US9, or both. The BAC DNAs were used to generate four viruses: GS2843, which expresses gE and US9; GS2843ΔgE, lacking gE; GS2843ΔUS9, lacking US9; and GS2843ΔgEΔUS9, lacking gE and US9. Western blot analysis demonstrated the loss of expression of gE, US9, or both (Fig. 6). In this experiment, the precursor form of gI (pgI) accumulated to higher levels in cells infected with the ΔgE or ΔgE ΔUS9 mutant, because pgI accumulates in the endoplasmic reticulum (ER) to a greater extent without the expression of gE (19, 41, 42). The replication of the mutant lacking gE, US9, or both was similar to that of the parental GS2843 virus (Fig. 7). However, it is important to note that all four recombinants (including GS2843, which expresses gE and US9) produced infectious progeny more slowly than wild-type HSV-1 strain F (Fig. 3). Maximal yields of GS2843 and derivatives were attained only after 30 to 32 h of infection, compared the maximal yields of infectious wild-type HSV strain F, which occurred before 24 h (not shown). This difference appears to be related primarily to the expression of mRFP-conjugated VP26, which slows HSV replication and the production of infectious virus in neurons (4, 10, 16). All four of these recombinant viruses began to lose the expression of mRFP-VP26 even after just 4 to 5 passages in Vero cells, supporting strong selective pressure against the production of the VP26 fusion protein that apparently compromises capsid assembly (data not shown). The loss of GFP-gB occurred during virus passage in Vero cells, but this was slower and rare.

Anterograde transport of fluorescent capsids and gB to axon tips and extracellular spread to other cells. These two-color HSV recombinants expressing fluorescent capsids and gB were characterized in terms of transport into distal axons. This was more difficult than for the HSV mutants described in the legend of Fig. 4, because the replication and axonal transport of the GS2843-derived viruses were substantially slower than those of wild-type HSV strain F. Moreover, there were fewer (~25%) gB and capsid puncta observed in distal axons than for wild-type HSV, illustrating the defects with these two-color viruses that we noted previously (16). In addition, GS2843-derived viruses were more toxic for neurons, axons began to peel off the glass substrate at later times, and it was more difficult to stain axons. However, in a series of experiments, we confirmed defects in axonal transport with these recombinants. Figure 8A shows mRFP-VP26 and GFP-gB puncta in distal axons (axonal compartments) 22 h after infection. Again, we detected not a single capsid or gB punctum with the $gE^-/US9^-$ double mutant strain GS2843ΔgEΔUS9 in four different experiments involving over 40 wells. We also compared capsids detected by staining with VP5-specific (large capsid protein) antibodies (Fig. 8B). Again, there were quantitative reductions in the numbers of capsids with gE^- and $US9^-$ mutants, but no capsids were detected with the $gE^-/US9^-$ double mutant compartments (Fig. 8B). The extracellular spread of HSV to adjacent Vero cells (plated in axonal chambers) was examined by staining Vero cells with ICP4-specific antibodies. We detected no $ICP4^+$ Vero cells in axonal compartments when neurons were infected with GS2843ΔgEΔUS9 (Fig. 8C). These results confirmed our results described above, showing that the loss of both gE and US9 abolished the transport of HSV capsids and glycoproteins to distal axons and spread to nonneuronal cells.

Anterograde transport of fluorescent capsids and gB in microfluidic chamber channels. To characterize the models for how gE/gI and US9 function, it was important to characterize the quality of anterograde transport of capsids and glycoproteins. Given that the $gE^-/US9^-$ double mutant transported many fewer capsids and gB puncta into distal axons, these two models could be more readily tested. SCG neurons plated in the somal compartments of microfluidic chambers were infected with GS2843, GS2843ΔgE, GS2843ΔUS9, or GS2843ΔgEΔUS9, and live-cell

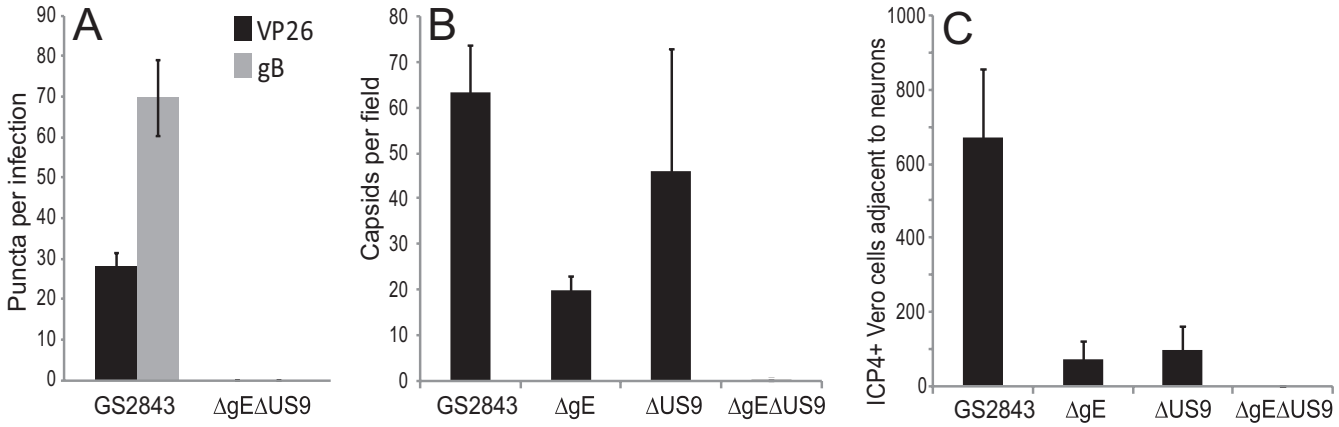

FIG 8 Capsids and gB in distal axons following infection with fluorescent HSV recombinants lacking gE, US9, or both, and virus spread to nonneuronal cells. SCG neurons were infected with GS2843, GS2843ΔgE, GS2843ΔUS9, or GS2843ΔgEΔUS9 at 5 PFU/cell in somal compartments and then incubated for 22 h. (A) Quantification of mRFP-VP26 and gB puncta in axons found in axonal compartments. (B) Methanol-acetone (1:1) at −20°C was added to somal compartments for 10 min, the devices were then disassembled, and axons were stained with anti-VP5 polyclonal antibodies and secondary fluorescent antibodies. (C) Vero cells were plated in axonal compartments, neurons were infected in somal compartments as described above, and after 22 h, the Vero cells were then stained with anti-ICP4 antibodies, as described in the legend of Fig. 5.

imaging of axons in microchannels was then performed. As in previous studies (16), we observed three types of fluorescent puncta, GFP-gB, mRFP-VP26-labeled capsids, and dual-color Married particles, although again, the majority of capsids were Separate particles. There were few capsids, glycoproteins, and Married particles present in axons of neurons infected with the gE-, US9-, and gE/US9-null viruses. At least 10 separate microchannels were imaged for each virus in 4 experiments, and there were few or no capsids or gB puncta in the majority of microchannels containing neurons infected with the ΔgE, ΔUS9, and ΔgE ΔUS9 mutants. In contrast, most microchannels containing axons of neurons infected with wild-type strain GS2843 displayed many capsids and gB puncta, and a fraction of these moved. Given the reduced numbers of capsids and gB puncta, we focused on comparing the ΔgE ΔUS9 double mutant with wild-type strain GS2843. Only capsids and gB that were moving during a significant portion of the 2-min observation window were counted, not puncta that remained stalled. GS2843-infected neurons exhibited a total of 123 moving puncta, including all of the gB, VP26 capsid, and Married puncta, in the 4 experiments, whereas GS2843ΔgEΔUS9-infected neurons displayed only 6 gB and 4 capsid puncta (Table 1). Nevertheless, these small numbers of capsids and gB puncta in axons of GS2843ΔgEΔUS9-infected neurons were significant compared to the complete absence of any detectable puncta in distal axons (Fig. 4 and 8).

TABLE 1 Summary of the anterograde transport of HSV puncta in live rat SCG medial neurons in microfluidic chambers

	No. of puncta					
	RFP-VP26/GFP-gB			ΔgE ΔUS9		
Expt	VP26 only	gB only	Married	VP26 only	gB only	Married
1	17	0	0	0	0	0
2	1	33	6	2	2	0
3	3	44	10	1	1	0
4	2	5	2	1	3	0
Total	23	82	18	4	6	0

Time-lapse movies for all three mutants and wild-type strain GS2843, capturing images every 2 s for 2 min, are shown in the supplemental material: GS2843 (Fig. S1 and S2), ΔgE (Fig. S3 and S4), ΔUS9 (Fig. S5 and S6), and ΔgE ΔUS9 (Fig. S7 and S8). The quality of some of these movies is relatively poor compared with our previous results (see the supplemental material in reference16). It must be kept in mind that there were very few capsids and gB puncta with these mutants. Still images derived from these movies are shown in Fig. 9. These studies demonstrated that both gB and capsid puncta moved at relatively normal speeds, 0.5 to 2.0 μm/s, in axons of ΔgE-, ΔUS9-, and ΔgE ΔUS9-infected neurons. In the movies (see Fig. S1 to S8 in the supplemental material), speeds were 1 to 2 μm/s, but there were other examples of puncta moving at speeds as low as 0.5 μm/s (not shown). Importantly, we did not observe increased stalling or retrograde transport of either capsids or gB puncta when we compared the ΔgE, ΔUS9, and ΔgE ΔUS9 mutants with wild-type strain GS2843. It should be kept in mind that there were very few puncta in axons of ΔgE-, ΔUS9-, and ΔgE ΔUS9-infected neurons, making a definitive characterization of the kinetics of this transport difficult. Together, these experiments showed that the $gE^{-}/US9^{-}$ mutant exhibited major reductions in the numbers of capsids, glycoproteins, and Married particles in medial axons, but the quality of this transport was not apparently different. Nevertheless, we detected some capsids and gB in medial axons, but not in distal axons, suggesting that there may be defects in transport in the axons themselves.

Transport of capsids and gB transport into proximal axons. Given the reduced numbers of HSV structural proteins in medial axons, it appeared that the loading hypothesis might explain most of the defects in transport associated with the loss of both gE and US9. Thus, it was important to determine whether viral proteins exited cell bodies and entered proximal axons. Live-cell imaging of neuron cell bodies and proximal axons was complicated by three factors. First, the somal chambers contained input virus as well as virus produced in cell bodies and shed into the medium,

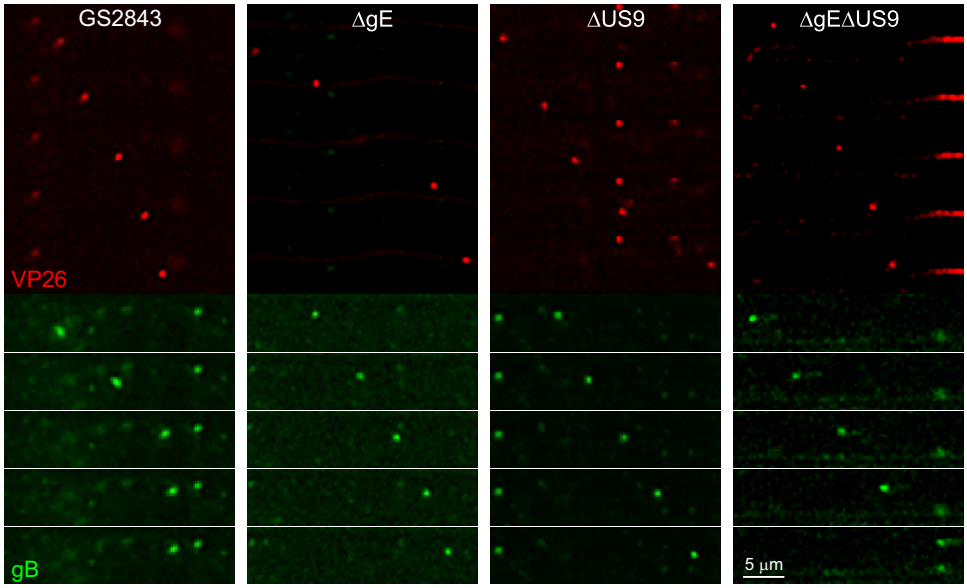

FIG 9 Sequential still images of medial axons derived from live-cell analyses. Images of mRFP-VP26 capsid puncta (red) or GFP-gB puncta (green) moving in neuronal axons were derived from live-cell imaging of axons in microchannels. Neurons were infected with GS2843, GS2843ΔgE, GS2843ΔUS9, or GS2843ΔgEΔUS9, and after 22 h, live-cell imaging was then performed on axons in microchannels. Still images taken 2 s apart of capsids or gB puncta are shown.

virus particles that stick back onto cells. Second, cell bodies produce large quantities of capsid and glycoprotein fluorescence that can obscure the much less intense fluorescence in axons. Third, SCG neuronal axons are long, and assigning which axons are derived from which cell bodies was frequently difficult. For these reasons, it was important to use live-cell analyses, to image capsids and glycoproteins that are moving anterograde from cell bodies into proximal axons. Figure 10, left, shows serial images taken every 2 s and derived from a movie (see Fig. S9 in the supplemental material) of a neuron infected with wild-type strain GS2843, focusing on the neuron cell body and proximal axon (defined by artificial white lines). This GS2843-infected neuron was at an earlier stage of virus replication, and mRFP-VP26 was largely concentrated in the nucleus, which was intentionally cropped out of this image, related to intense fluorescence. A Married particle (Fig. 10, white arrows) can be seen moving out of the cell body into the proximal axon. In the movie in Fig. S9 in the supplemental material, there were also several Separate capsids and gB puncta that moved into the proximal axon. Other axons of neurons infected with GS2843 showed similar transport into axons. Figure 10, right, shows a neuron infected with GS2843ΔgEΔUS9 that was in later stages of HSV infection and exhibited more capsids in the cytoplasm than the GS2843-infected neurons shown in the left panels. This neuron exhibited a major axon extending from the lower right corner of the cell toward the lower right side of the panel (defined by white lines). This axon was more difficult to discern by fluorescence, as viral proteins did not enter the axon, but the structure of the axon was readily seen by phase microscopy (not shown). There was no movement of fluorescent capsids or gB into the axon of this ΔgE ΔUS9-infected neuron. In addition, there were no obvious stalled capsids or gB puncta in this axon. Many other axons of ΔgE ΔUS9-infected neurons were characterized, and there were very few capsids or gB puncta found in the proximal axons, although, for the reasons described above, it was impossible to accurately quantify this. Figure S10 in the supplemental material shows movies of two ΔgE ΔUS9-infected neurons, one in an early stage of infection and one in later stages of infection. Again, no puncta were observed entering axons. We concluded that the majority of the defect in axonal transport associated with the loss of both gE and US9 involves an inability to transport capsids and gB into proximal axons.

DISCUSSION

There have been extensive studies showing that both gE/gI and US9 play important roles in HSV anterograde spread in the nervous systems of experimentally infected animals (24, 40, 43, 44). One important component of this spread involves anterograde axonal transport, a process that is entirely intracellular. Our previous studies described evidence that HSV gE/gI and US9 each contribute quantitatively to this first step in neuronal spread (4). Specifically, gE- and gI-null viruses displayed 5- to 10-fold reductions in the numbers of capsids and gB or gD puncta in more distal axons of human SK-N-SH neuroblastoma cells by staining glycoproteins or capsids with antibodies. Here, we used rat SCG neurons with much longer axons and grown in microfluidic chambers to isolate cell bodies from medial and distal axons, and detected gB and capsids with antibodies and using recombinant fluorescent proteins. Again, there were quantitative reductions in numbers of capsids and gB puncta in distal axons. Capsids were reduced to 5% in neurons infected with F-gE/GFP and to 29% in neurons infected with F-US9/GFP. gB puncta were reduced to 27% with F-gE/GFP and 46% with F-US9/GFP. A second set of mutants, ΔgE and ΔUS9, derived from GS2843 that expressed fluorescent capsids and gB produced similar observations. It was not surprising that HSV spread to Vero cells (plated in axonal chambers) was also reduced: F-gE/GFP infected 12% of the number of cells and F-US9/GFP infected 4% of the number of Vero cells compared with wild-type HSV. We concluded that both gE/gI and US9 significantly contribute to the axonal transport of HSV capsids and

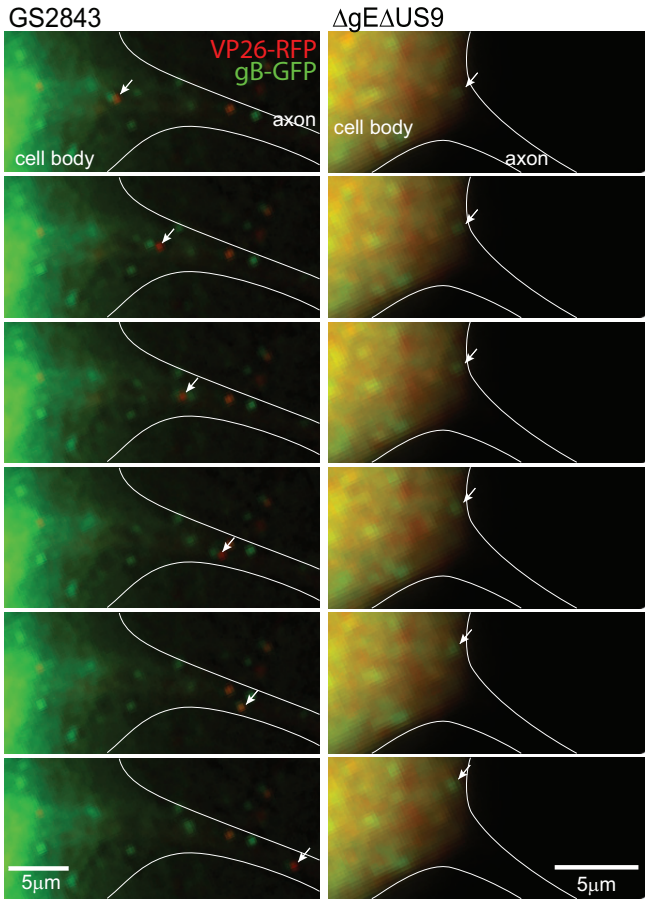

FIG 10 Sequential images of neuron cell bodies. Neurons were infected with HSV recombinant strain GS2843 or GS2843ΔgEΔUS9. Live-cell imaging of neuron cell bodies in somal compartments was performed, and still images (separated by 2 s) were derived from these movies. The left panels represent a neuron infected with GS2843 in an earlier stage of infection, with the majority of RFP-VP26 remaining in the nucleus, which was intentionally cropped out of these images, related to intense fluorescence. A Married HSV particle is shown moving from the neuron cell body into an axon initial segment. Note that live-cell imaging requires switching filters, which creates a small separation of red and green signals with Married particles. A Separate capsid was observed moving from this neuron cell body into the initial axon segment in Fig. S1 in the supplemental material. The right panels show a neuron infected with GS2843ΔgEΔUS9. This neuron was in a later stage of infection, when RFP-VP26 and GFP-gB were present at higher levels in the cytoplasm. With this neuron, there were no capsids or gB puncta that moved into axons.

glycoproteins, and there were reductions in spread to nonneuronal cells.

These conclusions fit well with extensive studies involving PRV gE/gI and US9. Enquist and colleagues showed that there were quantitative reductions in the numbers of capsids and glycoproteins, especially in more distal axons, and reduced spread from nonneuronal cells to adjacent cells (29, 30, 45, 46). Some of these studies indicated that PRV US9 is relatively more important than gE/gI, in terms of anterograde transport and spread. For example, a PRV US9$^-$ mutant was reduced by 10^4 to 10^5 in the quantities of infectious virus produced in adjacent nonneuronal cells, compared with wild-type PRV, whereas a PRV gE$^-$ mutant was reduced by 10^2 to 10^3 (30).

McGraw et al. (31) concluded that HSV US9 is not required for anterograde spread but that HSV gE/gI is required. As noted in the introduction, their conclusions were based on observations of virus spread to Vero cells relatively late after infection (48 h), when high virus titers reflect massive HSV amplification in Vero cells. At earlier times (24 h), titers produced by US9$^-$ mutants in these Vero cells were substantially reduced (31). We measured ICP4 expression in the first Vero cells that acquired HSV from neurons, showing that US9$^-$ mutants were substantially defective in spread to Vero cells. As noted above, spread involves (i) axonal transport, followed by (ii) extracellular spread from neurons to adjacent cells. The gE/gI heterodimer possesses large extracellular domains that can mediate an extracellular phase of HSV spread between epithelial cells (47). In recent studies, we genetically separated axonal transport and extracellular spread in studies involving gE extracellular domain mutants (P. W. Howard, unpublished data). In contrast, US9 does not possess an extracellular domain and, thus, cannot apparently participate in extracellular spread. Thus, there are dangers associated with comparisons of US9 to gE/gI when spread is measured. This problem can color studies done with experimental animals when the many steps of spread are combined. For example, in the retinal system, there is (i) spread within the retina, (ii) anterograde transport to the brain, and (iii) spread from optic neuronal axons to brain neurons, followed by (iv) spread between brain neurons.

Our observations with gE$^-$, US9$^-$, and gE$^-$/US9$^-$ mutants allowed us to address several important questions about how these HSV membrane proteins function. First, do gE/gI and US9 act in the same or different pathways to mediate axonal transport? For example, HSV gE/gI and gD function cooperatively or in a redundant fashion to promote secondary envelopment (33). Second, where in neurons (cell bodies versus axons) are the effects of these membrane proteins evident? Importantly, there were no observed HSV capsids and gB in distal axons (axonal compartments) with two different gE$^-$/US9$^-$ double mutants. Moreover, these double mutants did not spread to a single Vero cell plated adjacent to these neuronal axons. These results parallel studies with PRV vaccine strain Bartha that lacks both gE/gI and US9 and exhibits little or no anterograde transport and spread (13, 29), although Bartha also has other mutations. We concluded that HSV gE/gI and US9 act cooperatively or in an overlapping fashion to promote the anterograde axonal transport of both capsids and glycoproteins.

Imaging of capsids and gB puncta in proximal axons showed that HSV capsids and gB vesicles were rarely transported into proximal axons. Similar observations have been made with a PRV US9 mutant (45, 46). Together, these results largely supported the loading hypothesis. By this model, capsids and glycoproteins fail to be loaded onto kinesin motors and transported into proximal axons in the absence of both gE and US9. This fits with observations that HSV gE/gI and US9 accumulate in the TGN and that gE/gI interacts with other HSV membrane and tegument proteins (25–28). Thus, by serving to concentrate other viral proteins into TGN-derived vesicles that serve as platforms for loading onto kinesin motors, gE/gI and US9 might promote transport into proximal axons (Fig. 1A). Capsids are also extensively coated by tegument proteins, and thus, gE/gI and US9 might promote capsid loading onto motors, by interacting with these tegument proteins, as depicted in Fig. 1B. This model bears similarities with a model that we proposed for the gE/gI-mediated sorting of HSV particles in polarized epithelial cells (reviewed in references 2 and48). The TGN is also the major cytoplasmic site for the sorting of mem-

brane proteins to basolateral versus apical surfaces (reviewed in references 49 and50). HSV gE$^-$ mutants are missorted and not delivered to epithelial cell-cell junctions (51).

There is another mechanism that might explain the reduced numbers of HSV structural components that enter proximal axons. Axon hillock and axon initial segments (AIS) can act to filter membrane proteins, preventing transport down axons. For example, a dense actin network is formed in AIS, causing certain cellular cargo molecules to be retained at AIS, while other cargo, transported by different kinesins, bypass these filters (52). Our data might be explained by effects of gE/gI and US9 working at axon hillock or AIS to promote the transport of HSV cargo into proximal axons by either altering actin networks or bypassing these filters. Studies by Cunningham et al. (6, 7) and our studies (4, 10) showed that capsids and glycoproteins accumulate to high concentrations in neuron cell bodies until relatively late in infection (15 to 18 h), followed by relatively abrupt transport into axons. Perhaps, the effects of gE/gI and US9 involve overcoming filters or impediments to axonal transport.

The adaptor model (Fig. 1C) predicts that gE/gI and US9 function in axons to maintain interactions between kinesin motors and complexes of viral proteins. The relatively rare HSV puncta observed in medial axons were transported with normal velocities and without increased stalling, arguing against the adaptor model. However, not a single capsid or gB punctum was observed in distal axons despite imaging over 80 separate wells. Moreover, we did not detect a single infected Vero cell. These observations suggest that the few capsids and glycoproteins observed in medial axons failed to reach distal axons. These structures might fall off motors or stall at microtubule transfer points or in more distal axons in a manner which we could not observe. It should be kept in mind that the adaptor and loading models are not mutually exclusive. If loading onto motors in cell bodies is reduced, there might also be a reduced affinity of HSV proteins for motors within axons.

ACKNOWLEDGMENTS

We are especially indebted to Aurelie Snyder at the Advance Light Microscopy Core at the Jungers Center, OHSU, for her extensive efforts and skill in performing deconvolution and live-cell imaging. Todd Wisner contributed extensively to the design and implementation of these studies.

This work was supported by a grant from the National Institutes of Health, RO1 EY018755 (to D.C.J.).

REFERENCES

1. **Diefenbach RJ, Miranda-Saksena M, Douglas MW, Cunningham AL.** 2008. Transport and egress of herpes simplex virus in neurons. Rev. Med. Virol. **18**:35–51.
2. **Johnson DC, Baines JD.** 2011. Herpesviruses remodel host membranes for virus egress. Nat. Rev. Microbiol. **9**:382–394.
3. **Kratchmarov R, Taylor MP, Enquist LW.** 16 July 2012. Making the case: married versus separate models of alphaherpes virus anterograde transport in axons. Rev. Med. Virol. [Epub ahead of print.]
4. **Snyder A, Polcicova K, Johnson DC.** 2008. Herpes simplex virus gE/gI and US9 proteins promote transport of both capsids and virion glycoproteins in neuronal axons. J. Virol. **82**:10613–10624.
5. **Miranda-Saksena M, Armati P, Boadle RA, Holland DJ, Cunningham AL.** 2000. Anterograde transport of herpes simplex virus type 1 in cultured, dissociated human and rat dorsal root ganglion neurons. J. Virol. **74**:1827–1839.
6. **Penfold ME, Armati P, Cunningham AL.** 1994. Axonal transport of herpes simplex virions to epidermal cells: evidence for a specialized mode of virus transport and assembly. Proc. Natl. Acad. Sci. U. S. A. **91**:6529–6533.
7. **Saksena MM, Wakisaka H, Tijono B, Boadle RA, Rixon F, Takahashi H, Cunningham AL.** 2006. Herpes simplex virus type 1 accumulation, envelopment, and exit in growth cones and varicosities in mid-distal regions of axons. J. Virol. **80**:3592–3606.
8. **Negatsch A, Granzow H, Maresch C, Klupp BG, Fuchs W, Teifke JP, Mettenleiter TC.** 2010. Ultrastructural analysis of virion formation and intraaxonal transport of herpes simplex virus type 1 in primary rat neurons. J. Virol. **84**:13031–13035.
9. **Snyder A, Bruun B, Browne HM, Johnson DC.** 2007. A herpes simplex virus gD-YFP fusion glycoprotein is transported separately from viral capsids in neuronal axons. J. Virol. **81**:8337–8340.
10. **Snyder A, Wisner TW, Johnson DC.** 2006. Herpes simplex virus capsids are transported in neuronal axons without an envelope containing the viral glycoproteins. J. Virol. **80**:11165–11177.
11. **Antinone SE, Smith GA.** 2006. Two modes of herpesvirus trafficking in neurons: membrane acquisition directs motion. J. Virol. **80**:11235–11240.
12. **del Rio T, Ch'ng TH, Flood EA, Gross SP, Enquist LW.** 2005. Heterogeneity of a fluorescent tegument component in single pseudorabies virus virions and enveloped axonal assemblies. J. Virol. **79**:3903–3919.
13. **Feierbach B, Bisher M, Goodhouse J, Enquist LW.** 2007. In vitro analysis of transneuronal spread of an alphaherpesvirus infection in peripheral nervous system neurons. J. Virol. **81**:6846–6857.
14. **Maresch C, Granzow H, Negatsch A, Klupp BG, Fuchs W, Teifke JP, Mettenleiter TC.** 2010. Ultrastructural analysis of virion formation and anterograde intraaxonal transport of the alphaherpesvirus pseudorabies virus in primary neurons. J. Virol. **84**:5528–5539.
15. **Antinone SE, Smith GA.** 2010. Retrograde axon transport of herpes simplex virus and pseudorabies virus: a live-cell comparative analysis. J. Virol. **84**:1504–1512.
16. **Wisner TW, Sugimoto K, Howard PW, Kawaguchi Y, Johnson DC.** 2011. Anterograde transport of herpes simplex virus capsids in neurons by both Separate and Married mechanisms. J. Virol. **85**:5919–5928.
17. **Alconada A, Bauer U, Sodeik B, Hoflack B.** 1999. Intracellular traffic of herpes simplex virus glycoprotein gE: characterization of the sorting signals required for its trans-Golgi network localization. J. Virol. **73**:377–387.
18. **McMillan TN, Johnson DC.** 2001. Cytoplasmic domain of herpes simplex virus gE causes accumulation in the trans-Golgi network, a site of virus envelopment and sorting of virions to cell junctions. J. Virol. **75**:1928–1940.
19. **Wisner T, Brunetti C, Dingwell K, Johnson DC.** 2000. The extracellular domain of herpes simplex virus gE is sufficient for accumulation at cell junctions but not for cell-to-cell spread. J. Virol. **74**:2278–2287.
20. **Wisner TW, Johnson DC.** 2004. Redistribution of cellular and herpes simplex virus proteins from the trans-Golgi network to cell junctions without enveloped capsids. J. Virol. **78**:11519–11535.
21. **Brideau AD, Banfield BW, Enquist LW.** 1998. The Us9 gene product of pseudorabies virus, an alphaherpesvirus, is a phosphorylated, tail-anchored type II membrane protein. J. Virol. **72**:4560–4570.
22. **Brideau AD, del Rio T, Wolffe EJ, Enquist LW.** 1999. Intracellular trafficking and localization of the pseudorabies virus Us9 type II envelope protein to host and viral membranes. J. Virol. **73**:4372–4384.
23. **Brideau AD, Eldridge MG, Enquist LW.** 2000. Directional transneuronal infection by pseudorabies virus is dependent on an acidic internalization motif in the Us9 cytoplasmic tail. J. Virol. **74**:4549–4561.
24. **Polcicova K, Biswas PS, Banerjee K, Wisner TW, Rouse BT, Johnson DC.** 2005. Herpes keratitis in the absence of anterograde transport of virus from sensory ganglia to the cornea. Proc. Natl. Acad. Sci. U. S. A. **102**:11462–11467.
25. **Farnsworth A, Wisner TW, Johnson DC.** 2007. Cytoplasmic residues of herpes simplex virus glycoprotein gE required for secondary envelopment and binding of tegument proteins VP22 and UL11 to gE and gD. J. Virol. **81**:319–331.
26. **O'Regan KJ, Brignati MJ, Murphy MA, Bucks MA, Courtney RJ.** 2010. Virion incorporation of the herpes simplex virus type 1 tegument protein VP22 is facilitated by trans-Golgi network localization and is independent of interaction with glycoprotein E. Virology **405**:176–192.
27. **Stylianou J, Maringer K, Cook R, Bernard E, Elliott G.** 2009. Virion incorporation of the herpes simplex virus type 1 tegument protein VP22 occurs via glycoprotein E-specific recruitment to the late secretory pathway. J. Virol. **83**:5204–5218.
28. **Yeh PC, Han J, Chadha P, Meckes DGJ, Ward MD, Semmes OJ, Wills JW.** 2011. Direct and specific binding of the UL16 tegument protein of herpes simplex virus to the cytoplasmic tail of glycoprotein E. J. Virol. **85**:9425–9436.

29. **Ch'ng TH, Enquist LW.** 2005. Efficient axonal localization of alphaherpesvirus structural proteins in cultured sympathetic neurons requires viral glycoprotein E. J. Virol. **79**:8835–8846.
30. **Ch'ng TH, Enquist LW.** 2005. Neuron-to-cell spread of pseudorabies virus in a compartmented neuronal culture system. J. Virol. **79**:10875–10889.
31. **McGraw HM, Awasthi S, Wojcechowskyj JA, Friedman HM.** 2009. Anterograde spread of herpes simplex virus type 1 requires glycoprotein E and glycoprotein I but not Us9. J. Virol. **83**:8315–8326.
32. **Liu WW, Goodhouse J, Jeon NL, Enquist LW.** 2008. A microfluidic chamber for analysis of neuron-to-cell spread and axonal transport of an alpha-herpesvirus. PLoS One **3**:e2382. doi:10.1371/journal.pone.0002382.
33. **Farnsworth A, Goldsmith K, Johnson DC.** 2003. Herpes simplex virus glycoproteins gD and gE/gI serve essential but redundant functions during acquisition of the virion envelope in the cytoplasm. J. Virol. **77**:8481–8494.
34. **Park JW, Vahidi B, Taylor AM, Rhee SW, Jeon NL.** 2006. Microfluidic culture platform for neuroscience research. Nat. Protoc. **1**:2128–2136.
35. **Graham FL, van der Eb AJ.** 1973. Transformation of rat cells by DNA of human adenovirus 5. Virology **54**:536–539.
36. **Antinone SE, Zaichick SV, Smith GA.** 2010. Resolving the assembly state of herpes simplex virus during axon transport by live-cell imaging. J. Virol. **84**:13019–13030.
37. **Lee EC, Yu D, Martinez de Velasco J, Tessarollo L, Swing DA, Court DL, Jenkins NA, Copeland NG.** 2001. A highly efficient Escherichia coli-based chromosome engineering system adapted for recombinogenic targeting and subcloning of BAC DNA. Genomics **73**:56–65.
38. **Johnson DC, Frame MC, Ligas MW, Cross AM, Stow ND.** 1988. Herpes simplex virus immunoglobulin G Fc receptor activity depends on a complex of two viral glycoproteins, gE and gI. J. Virol. **62**:1347–1354.
39. **Georgopoulou U, Kakkanas A, Miriagou V, Michaelidou A, Mavromara P.** 1995. Characterization of the US8.5 protein of herpes simplex virus. Arch. Virol. **140**:2227–2241.
40. **Wang F, Tang W, McGraw HM, Bennett J, Enquist LW, Friedman HM.** 2005. Herpes simplex virus type 1 glycoprotein E is required for axonal localization of capsid, tegument, and membrane glycoproteins. J. Virol. **79**:13362–13372.
41. **Dingwell KS, Johnson DC.** 1998. The herpes simplex virus gE-gI complex facilitates cell-to-cell spread and binds to components of cell junctions. J. Virol. **72**:8933–8942.
42. **Hanke T, Graham FL, Lulitanond V, Johnson DC.** 1990. Herpes simplex virus IgG Fc receptors induced using recombinant adenovirus vectors expressing glycoproteins E and I. Virology **177**:437–444.
43. **Dingwell KS, Doering LC, Johnson DC.** 1995. Glycoproteins E and I facilitate neuron-to-neuron spread of herpes simplex virus. J. Virol. **69**:7087–7098.
44. **LaVail JH, Tauscher AN, Sucher A, Harrabi O, Brandimarti R.** 2007. Viral regulation of the long distance axonal transport of herpes simplex virus nucleocapsid. Neuroscience **146**:974–985.
45. **Lyman MG, Feierbach B, Curanovic D, Bisher M, Enquist LW.** 2007. PRV Us9 directs axonal sorting of viral capsids. J. Virol. **81**:11363–11371.
46. **Taylor MP, Kramer T, Lyman MG, Kratchmarov R, Enquist LW.** 2012. Visualization of an alphaherpesvirus membrane protein that is essential for anterograde axonal spread of infection in neurons. mBio **3**(2):e00063–12. doi:10.1128/mBio.00063-12.
47. **Polcicova K, Goldsmith K, Rainish BL, Wisner TW, Johnson DC.** 2005. The extracellular domain of herpes simplex virus gE is indispensable for efficient cell-to-cell spread: evidence for gE/gI receptors. J. Virol. **79**:11990–12001.
48. **Johnson DC, Huber MT.** 2002. Directed egress of animal viruses promotes cell-to-cell spread. J. Virol. **76**:1–8.
49. **Matter K, Mellman I.** 1994. Mechanisms of cell polarity: sorting and transport in epithelial cells. Curr. Opin. Cell Biol. **6**:545–554.
50. **Mostov KE, Verges M, Altschuler Y.** 2000. Membrane traffic in polarized epithelial cells. Curr. Opin. Cell Biol. **12**:483–490.
51. **Johnson DC, Webb M, Wisner TW, Brunetti C.** 2001. Herpes simplex virus gE/gI sorts nascent virions to epithelial cell junctions, promoting virus spread. J. Virol. **75**:821–833.
52. **Song AH, Wang D, Chen G, Li Y, Luo J, Duan S, Poo MM.** 2009. A selective filter for cytoplasmic transport at the axon initial segment. Cell **136**:1148–1160.